HEFAT2011
8th International Conference on Heat Transfer, Fluid Mechanics and Thermodynamics
26 June – 1 July 2011
Pointe Aux Piments, Mauritius

THE USE OF OPEN CELL METAL FOAMS IN HEAT EXCHANGERS: POSSIBILITIES AND LIMITATIONS

M. De Paepe*, H. Huisseune, P. De Jaeger, C. T'Joen
*Author for correspondence
Department of Flow, Heat and Combustion Mechanics
Ghent University- UGent
Belgium
E-mail: michel.depaepe@ugent.be

ABSTRACT

Open cell metal foam is under consideration for use in all kinds of heat transfer applications: electronics cooling, automotive heat exchangers, heat pumps, geothermal energy...

In order to design heat exchanger with this material, the foams need to be thermo-hydraulically characterized. Because of their interesting combination of properties (large specific surface area, tortuous flow paths, high strength…) a large amount of research has been done over the past decade. This paper will present a summary of this past research and indicate fields for further development. These are mainly due to issues with the complex foam geometry and how to characterize it adequately. Recently an advanced geometric model was developed at the Ghent University based on detailed micro-computed tomography scans of foam samples. Using this model it has been shown that for the hydraulic characterization the data spread can be reduced, by selecting the proper characteristic length scales. This is not only porosity; strut and cell dimension should also be included. Hydraulic analysis shows that applications with high fluid velocity are not intuitively favorable for foams. Low Reynolds-number forced convection and natural convection problems appear more interesting. However, by adapting the heat exchanger design to account for the pressure loss (e.g. foamed fins or thin foam layers), the advantages of foam can still be used at higher velocities. For thermal characterization little information is available. Experiments at the Ghent University, based on unsteady analysis have shown to give good results. These experiments have to be coupled with advanced numerical models of foams. Using these models, correlations for the combined conductive and convective heat transfer can be derived, which are needed to design and further optimize heat exchangers.

Open-cell metal foams clearly are a promising material for heat transfer technology. In order to see the first large scale use, specific applications will have to be selected and the heat exchanger designs will have to be optimized. Some examples are presented in the paper.

INTRODUCTION

Heat exchangers are critical components in the thermal management of transport, domestic and industrial applications, influencing safety, environmental quality and energy use.

Air is often the working fluid. The thermal convection of air is not high, resulting in an air-side thermal resistance which can be more than 80% of the total thermal resistance in most heat exchangers working with air. Consequently, reducing this air-side thermal resistance can result in substantial performance augmentation, yielding cost, space, material and energy savings.

Past research has led to considerable improvements by investigating the influence of fluid characteristics, flow arrangements, material selection and extending heat transfer surface area (through fins). In most forced convection applications, these heat transfer enhancement techniques aim to maximize the product of the heat transfer coefficient and heat transfer surface area per unit volume, whilst minimizing the air side pressure drop. Fins in different forms and lay outs are the current state of the art heat transfer enhancement techniques.

Further improvements aim to optimize the fin geometry, e.g. by adding vortex generators, or to replace the conventional fins with porous materials. Elaborating on the latter, a material that has drawn a lot of attention during past decades is open-cell metal foam. This material consists of a finite number of polyhedral cells, each encompassing a void. The voids are interconnected through pores, forming a single fluid space in the porous domain. The borders around a pore are termed struts and interconnect the nodes, forming a solid matrix which spans the entire porous domain. The introduced nomenclature is illustrated in Fig. 1.

Foam originates from the late 60's and is invented by the "Materials and Aerospace" division of Energy Research and Generation, Inc. (ERG). This had led to a major patent, explaining the manufacturing process in great detail [4]. The foams of ERG were intended for military and aerospace applications. Only since the mid 90's, the technology became available for non-classified military and industrial applications.

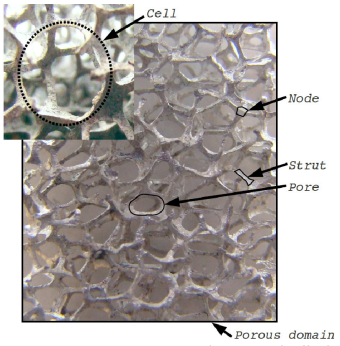

Figure 1 Foam nomenclature definitions

It explains why most literature on the subject is written only during the last decade, as can be seen in Fig. 2. The graph depicts the number of scientific publications per year, matching the search terms "foam", "PPI", "open-cell" and "heat transfer". Another indication of the technology release is that new manufacturers emerged since beginning 2000, like the German company M-Pore GmbH.

Open-cell metal foams are known to exhibit interesting structural and functional properties; the latter due to the open structure [1] :

- High porosity (> 0.85 when uncompressed)
- High interfacial surface area between the solid and fluid phase, per unit volume. This is also called surface-to-volume ratio. Typical values range from 400 to over 2500 m^{-1} when uncompressed.
- Relatively high strength and toughness, giving them structural stability Good impact energy absorption
- Good noise attenuation and impact energy absorption
- Excellent fluid mixing due to tortuous flow paths
- High gas permeability

A continuous disruption of the thermal and viscous boundary layer favours heat transfer between the solid matrix and fluid domain. This highly efficient way of heat transfer combined with a high interfacial surface-to-volume ratio and a highly thermally conductive solid material, makes open cell foams potential candidates for compact heat exchangers (CHEs). As depicted in Fig. 3a, Tian et al. [2] illustrated the attractive convective heat transfer characteristics of metal foams (and by extension of cellular metals) by making a comparison with louvered fins. However, disturbing boundary layers requires energy (i.e. pressure drop) which has to remain within the application specific operating conditions. Fig. 3b clearly illustrates that improved convective heat transfer comes at the expense of increased pressure drop. This is at once the biggest concern to apply open cell aluminum foam in CHEs.

OPEN-CELL ALUMINUM FOAM

Manufacturing of open-cell foams is done by either depositing the metal on a polymer precursor which is later removed or by replicating an organic template in the gestured metal via investment casting. The precursor removal in the first manufacturing process results in hollow struts, creating a significant structural difference between both methods [3]. This hollowness has implications for heat transfer, as it influences heat conduction in the solid matrix.

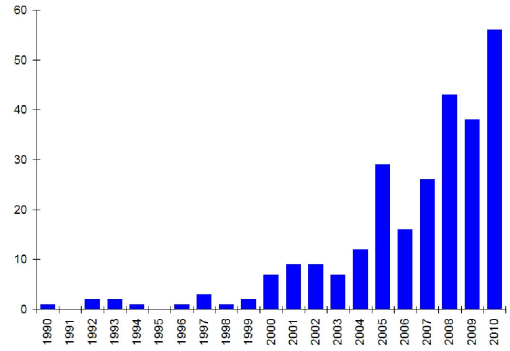

Figure 2 Annual number of publications since 1990, with a clear increase since 2000

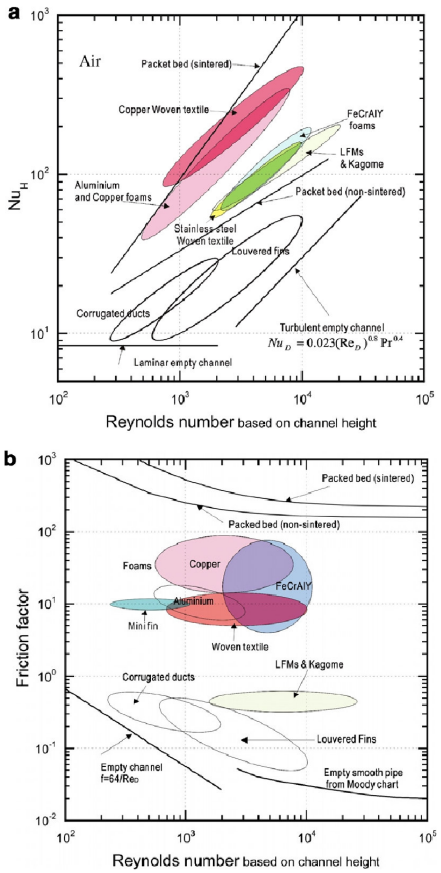

Figure 3 Comparison of various enhancement techniques: (a) Nusselt number as function of Reynolds number and (b) friction factor as function of Reynolds number [2]

The investment casting process is based on replicating a polymer preform; often a polyurethane open-cell preform [3]. The latter is manufactured in reactors, where polyurethane base material is subjected to a blowing agent under process dependent temperature and pressure profiles. The result of this foaming process is a closed-cell polyurethane foam, where cell faces are formed by a thin polyurethane film. Reticulating these closed-cell foams is done by blowing a hot gas through it,

which sublimates the faces. The result is a so called reticulated open-cell polyurethane foam, which acts as the preform for the metal foam. Prior to replicating the polyurethane foam, the struts can have an additional thickening. Consequently, cell- and strut dimensions can be controlled separately in the final template, which allows for tailoring the material for a specific application. The replicating process itself is an investment casting process, where the template is first filled with ceramics. Controlled heating allows the ceramics to harden. Additional heating results in the sublimation of the template, leaving the negative in the ceramics. Next the gestured metal is cast in this mould under vacuum conditions. After solidification, the mould is removed chemically and/or by high pressure spray and leaves a metal replicate of the template [4]. Figure 4 shows the result of two in-house cast foams, based on the same preform but with a different strut thickening process.

Besides manufacturing, there are two other major technological challenges upon foam can be used in thermal applications: (1) slicing of the foam to the desired dimensions and (2) bonding it on a substrate. Bonding is commonly done either by applying a highly conductive epoxy or by brazing. Epoxy bonding has the advantage of being readily available for research purposes, but results in an inferior thermal contact resistance, as can be concluded from Sekulic et al. [5]. The reason is the point-wise contact between foam struts and substrate and the breaking of the conductive path by even a thin layer of less conductive epoxy. Consequently, the contact surface area is minimal. This calls for a highly qualitative bonding like brazing, which is a metallic bonding.

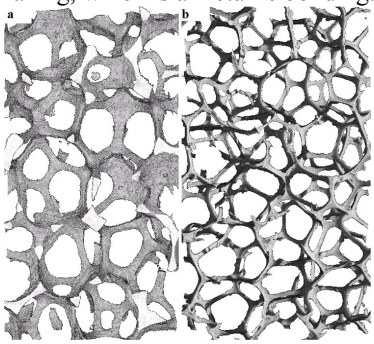

Figure 4 Two foams, manufactured with the same polyurethane preform but with (a) and without (b) strut thickening

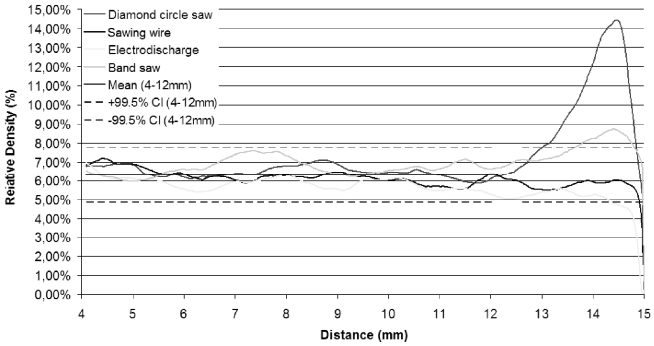

Figure 5 Porosity variation due to the plastic deformation during sawing, characterized for four methods

Aluminum brazing is commonly done on substrate material comprising a AA3000 Al-Mn alloy core, with a lower melting point AA4000 Al-Si alloy film on the brazing side(s). During brazing, a stacking of tubes and foam is heated past the Al-Si eutectic temperature (577 °C) of the brazing film. The core and foam material have a significantly higher melting temperature (liquidus 643 °C), preventing distortion of the final heat exchanger. With proper fluxing in a controlled atmosphere brazing furnace, the liquid brazing film establishes a joint between substrate and struts [6], if the spacing between them is within tolerance. Considering a typical tube wall thickness of 510µm, the required brazing film thickness is 50µm [6]. This gives an order of magnitude for the maximally allowed distance between substrate and foam in order to maximize the number of contact points.

Machining can result in plastic deformation of struts at the foam edges, creating local porosity variation [1] (see Fig. 5). Four 10PPI foam samples with the same bulk porosity are cut with four different tools. Next, the relative density of virtual slices parallel to the cutting edge (obtained via µCT scan), is plot against its position. The average relative density per slice is calculated for the bulk material (between 4-12mm), allowing to define 99.5% confidence levels. When relative density near the edges exceeds the confidence interval, it is considered to be abnormal and indicates where cutting influence is experienced. In the worst case (Diamond circle saw), this happens at 2 mm from the cutting edge, where the relative density can nearly double. This has a major impact on thermal and hydrodynamic characteristics near the solid-foam interface. When foam is cut at both sides of a slice, nearly 4 mm is influenced. Considering a slice thickness of 10 mm, this is a major disturbance.

Using a conventional band saw improves the slicing quality considerably. However, relative density still increases nearly 2%, compared to the bulk value of 6.38%. Perrot et al. [7] and Zhou et al. [8] took this issue in account and prepared their samples via electro-discharge machining. Virtually no plastic deformation is observed, but it results in a relative rough cutting surface as material is randomly removed by the discharge process. This is shown by the faster decay of the relative density when approaching the cutting edge. The consequence is a relatively larger distance between struts and a carrier, reducing the number of struts that make contact with the substrate. The least effect was obtained with sawing wire. It will ensure that a maximal number of struts make contact with a substrate.

GEOMETRICAL FOAM MODEL

Flow phenomena are inherently influenced by the geometry of objects the flow is passing. This has an impact on heat transfer and pressure drop as both the viscous and thermal boundary layer are altered. Consequently, it is mandatory to have an accurate description and dimensioning of the solid structure. This is the first task in order to study heat transfer with open-cell foams and is discussed in this section.

Foam Characterization

To characterize foam, manufacturers count the number of pores per linear inch (PPI) and report porosity Φ [-] or relative

density ρ_r [-] [9]. Because the structure of the foam is three-dimensional, the pores are not aligned along a single spatial coordinate, making PPI's more suitable for foam classification instead of a geometrical parameter [10]. Porosity is the ratio of the fluid phase to the total foam volume, commonly indirectly determined by measuring the foam's weight and specific density of the bulk material. A PPI-porosity combination is found inadequate to quantify the geometrical influence. T'Joen et al. [11] concluded this from their experiments on foam covered tube screens with different porosities. There was no conclusive correlation with porosity; rather a pore and strut dimension should be used. The same is concluded in Bonnet et al. [12], where effective hydraulic properties also correlate better with pore diameter than with porosity.

A third property is interfacial surface area A_{sf} [m²] between both phases, yielding the surface-to-volume ratio σ_0 [m^{-1}] when expressed per unit volume. It can be determined indirectly by measuring specific surface area (surface-to-mass ratio) via the Brunauer, Emmet and Teller (BET) method, i.e. a technique based on the gas adsorption/desorption at the interfacial surface area [13]. It measures the entire surface area, down to nanometer scale [14]. However, a nanometer scale analysis does not guarantee that the continuum assumption is valid. This can result in too large surface areas via the BET method for the intended analysis [14]. For example in air, a continuum analysis is allowed if the mean free path (±50nm) is 100 times smaller than a characteristic length of the geometry (or Knudsen number less than 0.01). This defines a valid length scale to measure geometrical parameters.

Another characterization method is micro-computed tomography scanning (µCT scan). A virtual, fully three-dimensional model of the foam's structure is reconstructed [15]. It allows determining the microscopical geometrical parameters (strut- and cell dimension) and the derived macroscopic properties (porosity and surface-to-volume ratio). The main difficulty is image segmentation; i.e. separating between solid and fluid phase. The voxels (3D pixels) which represent the solid-fluid boundary, generally consist of both phases. Such voxels span a large range of gray values. Segmentation is about setting the limit to categorize a gray value either as solid (1) or fluid (0). A solution is making the voxel size sufficiently small, as demonstrated in Fig. 6. The surface-to-volume ratio changed from 720 to 860m^{-1} for respectively the low and high resolution scan, making voxel size a major parameter when µCT scan data is used. Decreasing voxel sizes has revealed that surface-to-volume ratio converged asymptotically (Schmierer and Razani [10]).

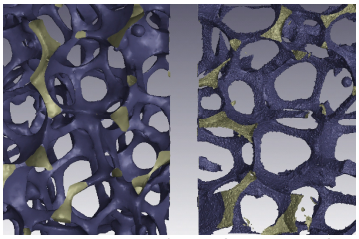

Figure 6 CT scan reconstruction of a 20PPI foam, from a low resolution scan (a) with 40µm voxel size and a high resolution scan (b) with 8.5µm voxel size

With the earlier introduced restriction for the continuum assumption to be valid, it is obvious that the high resolution scan can be considered most accurate. The drawback is that it can only be applied to a limited volume due to computer hardware restrictions.

It is worthwhile to mention scanning electron microscopy (SEM) analysis, as applied by Zhou et al. [8] and Tadrist et al. [16]. Foam samples are filled with a resin, i.e. cold mounting, and are subsequently polished. The polished side is reviewed under SEM, allowing performing image analysis.

A comparison of the three analysis methods is shown in Fig. 7, by evaluating surface-to-volume ratio. µCT results of five samples is added to literature data. Relatively good agreement is found between µCT and SEM data (Fig. 7). BET results however yield significantly higher σ_0 results, as is expected. For a continuum mechanics based analysis, high resolution µCT scan is most appropriate.

Foam Structure Representation

The most accurate foam model can be obtained via a virtual reconstruction from CT scan data. However, computational restrictions limit the volumes that can be analyzed. These are not sufficiently large for most problems, but are adequate to derive bulk properties for macroscopic analysis (see e.g. [17]).

Another approach is generating a model, based on the characteristic dimensions of the solid and fluid phase. A pore diameter is derived from the PPI count and used to approximate a strut length in a cubic cell representation of the solid matrix [18,19], see Fig. 8a. Struts are modelled as round, square or equilateral triangular rods. It is clear that this simplification requires a form of empiricism, to correlate bulk parameters to experimental data [18-20] because the small-scale geometrical features are not detailed enough. Consequently, results obtained via the cubic cell model can deviate substantially from experimental data (see e.g. Dharmasena and Wadley [21]).

The difficulty in modelling the foam structure is the stochastic nature and unidirectional cell elongation. Because of the latter, cells are characterized by the transverse (d_1 [m]) and conjugate (d_2 [m]) diameter of an ellipse encompassing the cell. Zhou et al. [8] and Perrot et al. [7] provide consistent data for both parameters. Perrot et al. [7] investigated the influence of cell elongation on the thermal characteristic length, calculated as twice the fluid-phase volume divided by the phase interfacial surface area. It revealed a significant difference of 30% between an isotropic and orthotropic cell model. Despite this improvement, there is still another 30% deviation compared to experimental data obtained via µCT. The reason has to be sought in the strut representation and will be discussed later.

The coefficient of variation (CV) on both cell diameters is only 5%, revealing a high degree of regularity in the structure. Thus foam is microscopically heterogeneous, but homogeneous on a macroscopic scale. This allows to represent the foam as a periodic reproduction of a unit cell; at least when a macroscopic analysis is intended or for the derivation of macroscopic properties.

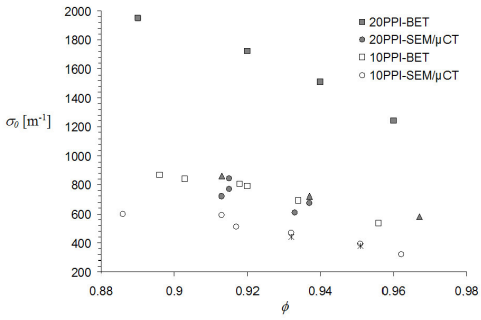

Figure 7 Surface-to-Volume ratio data for 10 and 20PPI foams, measured via BET [13], SEM [16], μCT scan from literature [7,10]. Notice the large deviation of the data obtained via BET

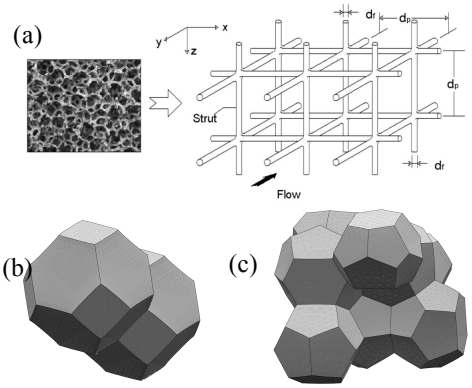

Figure 8 Periodic Unit Cell representations of foam. (a) Cubic cell [22], (b) Kelvin model and (c) Weaire-Phelan model [23].

A deterministic approach to obtain a periodic unit cell (PUC) representation is based on minimizing the total film energy of a closed-cell foam. The resulting wire-frame is a PUC of open-cell foam. The program "Surface Evolver" [24] is developed to solve this minimization problem. It is found that relaxing a Voronoi tessellation, with the seeds placed on a BCC lattice, yields the well known Kelvin cell (see Fig. 8b). A 0.03% more efficient unit cell was found by Weaire and Phelan [23], after relaxing a space partition with seeds placed on an A15 lattice (see Fig. 8c).

The averaged cell volume and diameter of the deterministic cells is found to be in close agreement with the values of the original structure [25]; despite they do not show the natural tendency to mainly form pentagonal faces [26] or orthotropicity or account for the stochastic nature. For analysing fluid flow related problems, a single-cell PUC predicts pressure drop and even turbulence levels within 5% accuracy [27]. Aiming at a computationally efficient model, the selection of such a PUC is valid; of course under the restriction that a macroscopic analysis is intended. Analysis of the microscopic heterogeneous behaviour in foams requires either a μCT scan or stochastic tessellation model (e.g. via Laguerre tessellation [28]).

The strut shape can be modelled independently and placed on a wire-frame representation of the foam. Using cylindrical or equilateral-triangular struts resulted in a variation of the characteristic thermal length in the order of the deviation between isotropic and orthotropic cell representation.

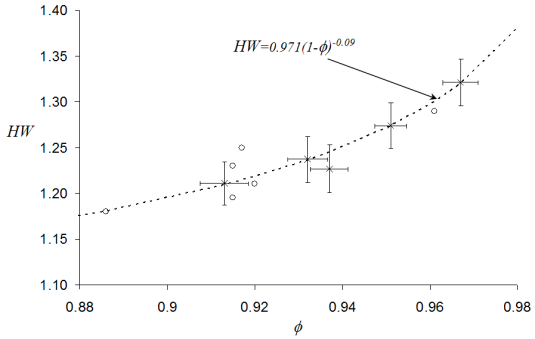

Figure 9 The porosity (Φ) depending Heywood circularity factor (HW) of five in-house manufactured foams (x) is added to the available data from literature (o) [10].

The importance of strut geometry in fluid dynamics is endorsed by the study of Hutter et al. [27]. A large eddy simulation on isotropic foam models for varying strut thicknesses and shapes indicated that these parameters are needed to quantify the ability of foam to act as static mixing element, even revealing the existence of an optimum. Also for effective thermal conductivity, the strut size variation was found to be significant. Kanaun and Tkachenko [29] analyzed this and concluded that the strut cross-sectional strut area in the middle between two nodes was a critical parameter.

Various definitions can be found to quantify the strut cross-sectional size, such as the average length of an edge [8], height of the best fitting equilateral triangle [7] [30], equivalent diameter of a circle yielding the same surface area or the hydraulic diameter [10]. However, depending on the thickening process of the polyurethane preform, the strut cross-sectional shape can vary from concave triangle with rounded tips to circular. Measuring on such shapes with axial size variation is prone to erroneous readings up to a factor two [31]. It is found more convenient to measure the strut cross-sectional surface area A_0 [m^2], which can be obtained directly from μCT data.

Strut cross-sectional shape depends on porosity [19], and clearly is not an equilateral triangle or a circle. This can be quantified via the Heywood circularity factor (HW), defined as the ratio of the strut cross-section perimeter to the equivalent perimeter of a circle with the same surface area. Fig. 9 depicts the porosity correlation of HW for five in-house manufactured foams (with 95% confidence level interval) and data from [10].

Strut axial shape variation is the last item to quantify. Kanaun and Tkachenko [29] assumed a parabolic axial shape. A more detailed study of was carried out by Jang et al. [32]. Three aluminum foams with nearly equal porosity were analyzed by means of CT scan. The result is reproduced in Fig. 10a. The averaged and normalized axial cross-sectional area variation $f(\xi)=A(\xi)/A_0$ seems independent of foam type (PPI) and behaves quartic. Expanding this data with foam porosities covering a range between 0.91 and 0.98 allows defining a general expression:

$$f(\xi)=a_2\,\xi^4+\xi^2+1, \qquad \text{with } \xi=x/l \text{ and } -l/2<x<l/2 \qquad (1)$$

The axial shape factor a_2 correlates with porosity, as is depicted in Fig. 10b.

Placing the described struts on the earlier introduced PUC representation of the foam cells allows constructing the final unit cell. Implementation in the pre-processor of a commercial CFD software package (Gambit®) can be done via so called journal files, allowing the creation parametric structures. Fig. 11 depicts an exemplary structure, generated with the earlier discussed strut shape correlations, for a given set of cell diameters and strut cross-sectional surface area. The resulting porosity and surface-to-volume ratio is found to be within measurement accuracy obtained via µCT scan (or within 8%).

For reasons of clarity, the model approximations are summarized here:

1. The stochastic nature of the foam is neglected, making it only applicable for macroscopic studies. It does not allow investigating the microscopic heterogeneity.
2. A constant cross-sectional strut shape is assumed along the axial position between two nodes which are interconnected by a strut.

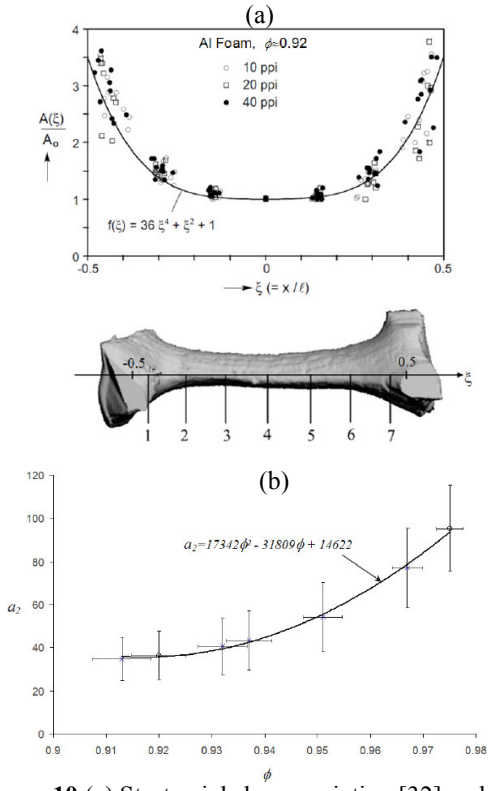

Figure 10 (a) Strut axial shape variation [32] and (b) correlation of shape factor a_2 with porosity Φ

THERMAL AND HYDRODYNAMIC ANALYSIS

The three-dimensional, complex solid structure of open-cell metal foams, results in very complicated flow phenomena below sub-cell scale. On the other hand, foam volumes are commonly two orders of magnitude larger, spanning a vast number of cells. The resulting multi-scale problem (spatially, as well as temporarily) is challenging, as sub-cell scale phenomena need to be transported to the engineer's designs scale. Three major analysis methods can be distinguished for the analysis of foam.

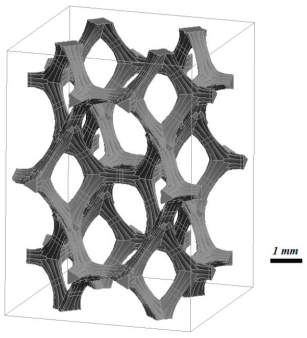

Figure 11 Generated PUC, with strut shape defined via the introduced correlations

1. Black-Box Approach

Idealizing the heat transfer allows to use a thermodynamic "black-box" approach. In steady-state, measuring heat flux and accompanying temperature difference allows to calculate an overall thermal resistance of the system. By subtracting the known resistances, all microscopic phenomena can be lumped in a heat transfer coefficient. Performing measurements for a variety of operating conditions and geometrical configurations allows correlating thermal performance. An example is a Colburn j correlation for louvered fins mounted between flat tubes, and given by [36]:

$$j_{fin} = \mathrm{Re}_{lp}^{-0.49}\left(\frac{\theta}{90}\right)^{0.27}\left(\frac{p_f}{l_p}\right)^{-0.14}\left(\frac{b}{l_p}\right)^{-0.29}\left(\frac{W_t}{l_p}\right)^{-0.23}\left(\frac{l_l}{l_p}\right)^{0.68}\left(\frac{p_t}{l_p}\right)^{-0.28}\left(\frac{\delta}{l_p}\right)^{-0.05} \quad (2)$$

The geometrical fin parameters are made dimensionless via the louver pitch l_p and an angle of 90 degrees for louver angle. The precise meaning of all the geometrical parameters can be found in [36]. The operating conditions are accounted for via the Reynolds number. The validity of the correlation is given for a range of fin geometrical parameters and operating conditions. Following Shah and Sekulic [33] however, there is also the influence of the flow arrangement. This is generally a uniform flow, normal to the heat exchanger core, and hereafter referred to as two-dimensional. The proposed correlation is valid for this one flow arrangement, which covers the majority of the intended applications with this fin type.

A similar correlation could be proposed for metal foam in the 2D flow arrangement:

$$j_{foam} = \mathrm{Re}_{d_2}^{c1}\left(\frac{d_1}{d_2}\right)^{c2}\left(\frac{\sqrt{A_0}}{d_2}\right)^{c3}(HW)^{c4}(a_2)^{c5}\left(\frac{W_t}{d_2}\right)^{c6}\left(\frac{b}{d_2}\right)^{c7}\left(\frac{L}{d_2}\right)^{c8} \quad (3)$$

with d_1, d_2, A_0, HW and a_2 the earlier introduced foam geometrical parameters. Tube thickness is represented by W_t, foam thickness between two flat tubes measures b and flow depth through the foam is resembled by L. The coefficients c1…c8 have to be obtained by fitting the proposed correlation to experimental (or numerical) data. It is clear that a vast number of data points are needed to solve this problem and would only cover the 2D flow arrangement. As foams are quasi-isotropic (compared to fins), they can also be used in 3D flow arrangements. This would result in more complex correlations, needing even more experiments.

Recalling that there is no clear consensus on the definition of the foam geometry, it is to be expected that a variety of heat transfer correlations can be found in literature, as depicted in

Fig. 12 (a). Furthermore, a multitude of characteristic lengths for the flow phenomena in foam can be found in literature:

- Equivalent particle diameter, which is a diameter yielding the same interfacial surface area per unit volume of solid material [42]. A slightly modified version is proposed by Dukhan and Patel [43], where the reciprocal of the surface-to-volume ratio is used.
- Average pore diameter, which can be measured relatively easy, provided it is well-defined [12,44].
- Strut diameter, assuming cylindrical struts. It is found by either dividing the solid volume with the total strut length [45] or determining the equivalent diameter of a circle yielding the same cross-sectional surface area of the strut.
- Strut thickness, which is determined as the side or height [30] of the strut's equilateral triangular cross-section
- Square root of permeability, which is a measure for the boundary layer thickness in packed bed of spheres [46]. Nevertheless, it is also often used for foams, see e.g. [47].
- Hydraulic diameter based on porous volume, calculated as four times the void volume per interfacial surface area [48].

The results presented in Fig. 12 and 15 were recalculated for Reynolds number based on equivalent strut diameter, all for a rectangular channel flow arrangement.

Another major influence is sample size variation. Salas and Waas [41] gave experimental justification for this observation by analyzing convective heat transfer through with foam for channel height varying from 6.4 to 25.4 mm, as shown in Fig. 12 (b). The relative influence of the solid foam boundaries is largest for smaller foam height.

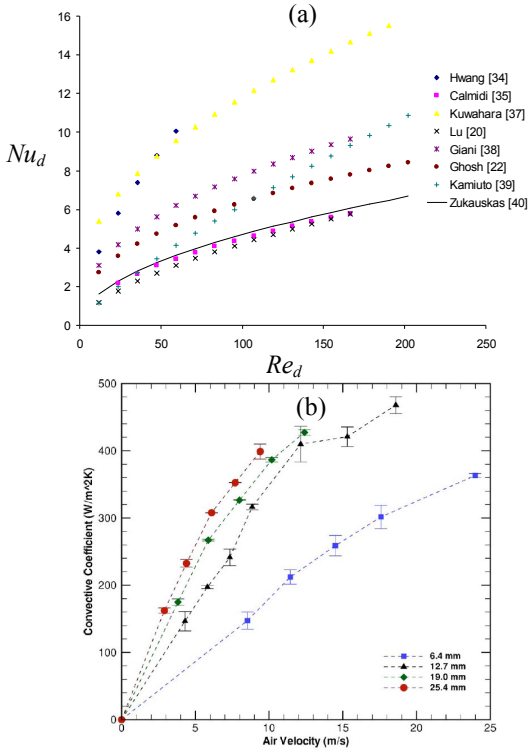

Figure 12: (a) Nusselt number variation for open-cell aluminum foams and (b) influence foam channel height [42].

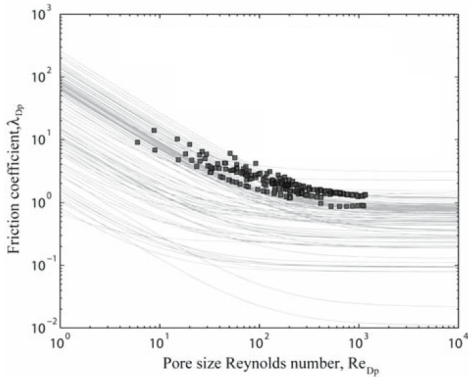

Figure 13: Friction factor review of available correlations, reproduced from [12]

Above 12.7mm, the influence is much less. Dukhan et al. [49,50] experimentally showed that the temperature of the solid matrix decays like the complementary error function, when the distance to the heater base is increased. They found that for 15 and 40 mm above the heated base (depending on the foam type and flow regime), the temperature of the solid matrix and cooling air becomes equal. Thus a limited foam height is effective [51]. This suggests a strong influence of the effective thermal conductivity, which will be dealt with later.

Ghosh [22] used the fin efficiency concept to take the limited effective thermal conductivity in account. For a 10mm foam layer and 1.5 m/s air velocity, the fin efficiency is 0.78. As a comparison, fin based CHEs for automotive and other applications, typically have minimum design fin efficiencies 0.89 [52]. To increase the fin efficiency of foam heat sinks, the insertion of longitudinal fins [53] or elliptic pin fins [54] has been investigated. It decreases the conductive path through the foam. The resulting heat transfer enhancement is a factor 1.5 to 2, at a given pressure drop.

In a black-box approach, thermal performance is often weighted with pressure drop to construct a performance evaluation criterion. A friction factor correlation is commonly used for fins applied in a 2D flow arrangement and are based on well known geometrical parameters, predicting pressure drop with sufficient accuracy. For foams however, various friction factor correlations are published, with various definitions of geometrical parameters. Bonnet et al. [12] made a database of the available data, showing large scatter (see Fig. 13). Besides the ambiguity in geometrical representation of the foam (and thus the associated characteristics), five other factors impact friction coefficient and are discussed more in detail in the local volume averaging section.

2. Direct Numerical Simulation

Instead of lumping all geometrical parameters and operating conditions into a series of heat transfer coefficients, it is possible to solve the classical conservation laws directly on the foam structure. Boundary conditions on the solid-fluid interface, as well as on the boundaries of the foam volume have to be applied. When the conventional Navier-Stokes and energy equations are solved, it is assumed that the continuum hypothesis holds.

Hugo et al. [17] performed an analysis on a virtual foam representation via µCT scan with the cubic sample having 15 mm as side length (foam type: 20PPI, with ϕ=0.92 and average cell diameter 4.5mm). Knowing that this simulation is done in steady state, it illustrates the computational limitations (assuming that the solution converged sufficiently and is grid independent). For practical applications, the order of magnitude of the foam volume is at least two orders of magnitude smaller larger than required. This can also be concluded from a direct simulation on a Weaire-Phelan structure with struts represented by rods with equilateral-triangular cross-section [30]. They succeeded in solving the conservation laws for a foam volume of 10 cells. For the unsteady turbulent flow phenomena, a k-ε turbulence model was used instead of performing an unsteady simulation.

Although computing power is increasing at a tremendous pace, solving conservation laws directly on a given geometry will stay applicable only for a limited number of cells in coming years. Thermal and hydrodynamic analysis for larger problems requires an intermediate method, between a black-box approach and a direct numerical simulation.

3. Local Volume Averaging

Fluid flow is commonly analysed on a continuum scale, which has to be at least two orders of magnitude larger than the molecular length and time scale (i.e. the Knudsen number for gasses). The phenomena occurring on molecular scales are then transported to the continuum transport equation via well known properties like viscosity and thermal conductivity. As these continuum scales in simulations still are out of reach for solving thermal and hydrodynamic problems in foam on a design scale, further up-scaling is required. A schematic representation of this problem is given in Fig. 14.

In this 2D representation, length scales are associated to the solid phase (d_s) and fluid phase (d_p). Averaging the continuum scale phenomena has to be done in a volume which makes statistical averaging meaningful, represented by the REV with length scale r_0. The REV's centroid position is indicated by vector $\vec{x}$ and absolute local position in the porous media is resembled by vector $\vec{r}$. Physical quantities are averaged inside the REV and appointed to the centroid. Sweeping the REV through the porous domain results in a new continuous field, with averaged continuum scaled phenomena.

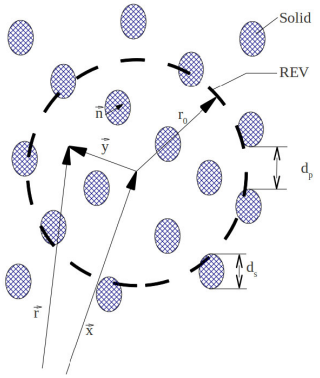

Figure 14: Length scales in the up-scale problem from continuum to porous media scale

This averaging acts as filtering high spatial frequency components with the REV being the filter. Filtering a quantity ψ is mathematically represented by following integral:

$$\langle \psi \rangle_{\vec{x}}^{s} \equiv \frac{1}{V_{REV}} \int_{V_{REV}} \psi(\vec{r}) dV \,, \qquad (4)$$

where the superscript s denotes superficial average and is considered over the total REV volume V_{REV}. An intrinsic average is obtained by integrating over a single phase and denoted with superscript i. The motivation to define two averages is that experimental data is typically obtained for one type, while it is difficult to measure the counterpart. For example intrinsic averaged pressure is measured in a porous medium, while velocities are easier expressed in a superficial average, i.e. volumetric flow divided by cross-sectional surface area. When generalizing the filter operator, it can be expressed as a convolution. This is a mathematical expression of sweeping the REV through the porous domain.

Averaging the Momentum Equation

Following Whitaker [57], filtering the classical Navier-Stokes equations for Newtonian and incompressible flow results in:

$$\begin{aligned} \rho_f \frac{\partial \langle \vec{v} \rangle^s}{\partial t} + \rho_f \nabla \cdot \left[\frac{\langle \vec{v} \rangle^s \langle \vec{v} \rangle^s}{\phi} \right] &= -\phi \nabla \langle P \rangle^i + \mu \nabla^2 \langle \vec{v} \rangle^s + \phi \rho_f \vec{g} \\ -\rho_f \nabla \cdot \left\langle \tilde{\vec{v}} \tilde{\vec{v}} \right\rangle^s &+ \frac{1}{V_{REV}} \int_{A_{sf}} \vec{n}_{fs} \cdot \left[-\tilde{P} \boldsymbol{I} + \mu \nabla \tilde{\vec{v}} \right] dA \end{aligned} \,, \qquad (5)$$

with ρ_f [kg/m^3] fluid density (with subscript f denoting fluid phase), $\vec{v}$ [m/s] velocity, t [s] time, P [Pa] pressure, μ [Pa.s] dynamic viscosity, $\vec{g}$ [m/s²] gravitational acceleration, $\vec{n}_{fs}$ [-] the normal vector on the fluid-solid interface and $\boldsymbol{I}$ the unit tensor. It is important to review the constraints, imposed to obtain this equation. Therefore, the pointwise values inside a REV are decomposed into an average value $<\psi>$ and its local deviation $\tilde{\psi}$. It is assumed that the averaged field is well-behaved, or $<<\psi>>=<\psi>$. For this, a length scale constraint is imposed: $r_0/L_\psi << 1$, with L_ψ a characteristic length of the gradient of the averaged quantity $<\psi>$ inside the REV. Recalling that the averaged field is continuous, it can vary inside a REV. Accounting for this variation inside a REV is a non-local transport phenomena or evolving heterogeneity, which is extremely complex to analyse [57]. Therefore, the imposed constraint simplifies the problem considerably.

Equation (5) is obtained by imposing the length scale constraint on the averaged pressure and velocity field, restricting spatial variation. Additional constraints on the REV size depend on whether or not the porous material is ordered. Recalling the validity of a PUC representation of the foam structure when a macroscopic analysis is intended, the periodic structure is inherently ordered. The appropriate filter size constraint is that the REV has to be equal to a single cell. Notice that a smaller REV size makes it easier to fulfil the introduced length scale constraint. When a stochastic foam model is needed (for example when foam is compressed, which makes the foam microscopic heterogeneous), the appropriate filter size constraint is that the REV size has to be larger than a cell. This is confirmed by Brun [58], where it was found that at least two cells are needed as REV size when the foam is

represented by µCT scan reconstruction. When a fully random structure is averaged, at least ten cells are required [57].

The last three terms in equation (5) depend on the local variation inside the REV. These terms transport the continuum-scale phenomena (i.e. sub-REV or microscopic scale) to the macroscopic scale of the up-scaled equation. To close this equation, these terms need to be related to the averaged quantities. These terms represent momentum dispersion inside the REV (4th term on r.h.s), a form drag term determined by the local pressure variation on the solid-fluid interface (first term of the integral on r.h.s.) and the viscous friction resulting from the no-slip condition at the interfacial surface (second term in the integral on r.h.s.).

Subtracting the volume averaged form from the continuum-scale equations yields a transport equation of the local variations. For the momentum equation, Whitaker [59] proved that closing the drag forces results in Darcy's law with Forchheimer correction. For the momentum dispersion term, a Fickian diffusion is proposed, where the geometry depending local mixing inside the REV is transported to the macroscopic scale via an effective viscosity $\underline{\underline{\boldsymbol{\mu}^e}}$. Although this approach resembles turbulence modelling, where an eddy viscosity is introduced, it should be stipulated that the introduced effective viscosity originates from forcing a fluid through the solid matrix instead of Reynolds stress. Therefore, to make the distinction, it is also termed mechanical dispersion. The final diffusion gradient-type model appearing in the averaged momentum equation is also referred to as the Brinkman correction term. This yields the well known continuity and momentum equation for porous media:

$$\begin{aligned} \nabla \cdot \vec{v} &= 0 \\ \rho_f \frac{\partial \vec{v}}{\partial t} + \frac{\rho_f}{\phi}\vec{v}\cdot\nabla\vec{v} &= -\phi\nabla P + \underline{\underline{\boldsymbol{\mu}^e}}\cdot\nabla^2\vec{v} - \mu\underline{\underline{\boldsymbol{\kappa}}}^{-1}\cdot\vec{v} - \rho_f\underline{\underline{\boldsymbol{\beta}}}\|\vec{v}\|\cdot\vec{v} \end{aligned} \quad (7)$$

The superscripts *s* and *i* are omitted for reasons of clarity. Three porous properties are introduced, which transport continuum-scaled phenomena to the macroscopic scale. The second term on r.h.s. is the Brinkman term and influences boundary layer formation in the porous volume near a no-slip or free flow condition. The third term is Darcy's law, accounting for the viscous friction at the solid-fluid interface via the permeability $\underline{\underline{\boldsymbol{\kappa}}}$. The continuum scaled counterpart is known as Stokes law. Last term is the Forchheimer correction, which accounts for inertial effects inside the solid structure or the form drag of the struts. The solid geometrical influence is captured with the inertial coefficient $\underline{\underline{\boldsymbol{\beta}}}$. Note that all three introduced properties have tensorial character, allowing to capture the orthotropic structural influences of foam.

Permeability and Inertial Coefficient

To determine the permeability and inertial coefficients, a one-dimensional windtunnel experiment is often conducted. Both hydrodynamic properties are derived by relating the measured pressure drop and superficial velocity according Forchheimer's law. For an alignment in x-direction, it reads:

$$\frac{\Delta P}{L} = \mu\kappa_{xx}^{-1}v_x + \rho\beta_{xx}v_x^2, \quad (8)$$

with L representing the flow length through the foam. Care should be taken as the obtained data can be influenced by (1) solid boundaries encompassing the foam, (2) entrance and exit effects (3) edge effects due to sample preparation (as shown above), (4) misalignment of velocity direction and cell orientation in anisotropic structures as afore mentioned, and (5) air compressibility. Bonnet et al. [12] made a comprehensive review of the available data in open literature, indeed revealing a scatter of nearly two orders of magnitude for the inertial coefficient. By emphasizing on accuracy, new experimental data of Bonnet et al. [12] showed a proportional relation of κ and β with respectively the square and the inverse of the pore diameter. Other correlations have been proposed to understand the influence of geometrical parameters on the hydrodynamic properties. A review is given by Mahjoob and Vafai [60] and by Edouard et al. [31].

Magnico [45] numerically determined both the permeability and Forchheimer tensors. The Darcy regime is found for $Re_d < 1$. The equivalent strut diameter was taken as characteristic length for the Reynolds number. Steady laminar inertial regime occurs between $1 < Re_d < 21$.

Plotting the Darcy and Forchheimer contribution of equation (8) reveals that this happens when both contributions are equal, as can be seen in Fig. 15. Above $21 < Re_d$, unsteadiness is introduced. Seguin et al. [61] used electrochemical probes to measure locally inside the cells and reported that the onset of turbulence was observed at Re_p equal to 290 and 350 for respectively a 10 and 20 PPI foam. This Reynolds number is determined with pore diameter as characteristic length. Recalculating for an equivalent strut diameter yields $Re_d = 60$ for the 10PPI foam. Following the general approach of Hlushkou and Tallarek [62], fully turbulent flow is considered when the Forchheimer contribution reaches 95% in equation (11). This is demonstrated in Fig. 15 for a 10 PPI foam with 0.94 porosity.

Recently, Dukhan and Minjeur [63] found that, based on experimental data, a different permeability should be defined depending on either the Darcy or Forchheimer flow regime. This was obtained for three foam types having a squared cross-section measuring 10.16 cm. Superficial air velocity was varied from 0 to 20 m/s. It is unclear if in this case, the solid wall confining the foam sample, has a significant contribution. A study of Innocentini et al. [64] for another configuration indeed suggests this possibility.

Numerical analysis of Magnico [45] on the other hand revealed that both permeability and inertial coefficient tensors show no dependency on Reynolds number. In fact, when the studied nickel foam is deformed by shearing it, the angle between the eigenvectors of both tensors and flow direction is found equal to the shear angle.

This makes the author conclude that both properties are material properties. Concerning the difference in magnitude between longitudinal and transverse cell orientation, 8 and 40% is found for respectively a non- and sheared foam. Clearly, cell orientation has a major influence on both hydrodynamic properties.

In forced convection applications, the Reynolds numbers are commonly above 10, making pressure drop depend on both the Darcy friction and Forchheimer inertial loss terms.

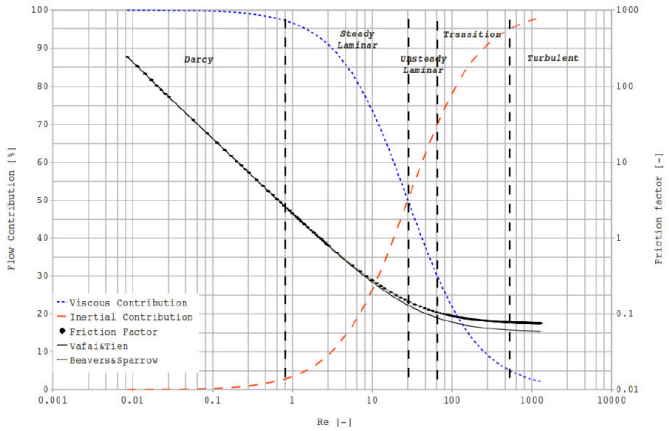

Figure 15: Viscous and inertial contribution versus Re (based on equivalent strut diameter) for a 10PPI, 0.94 porosity foam. Measured friction coefficient is shown and compared with data from literature, revealing good resemblance.

The latter term finds it origin in pressure difference across the interfacial surface area, especially the difference on the front pressure build up and lower pressure in the wake behind a strut. Comparing with fins however, the number of frontal and wake zones is considerable less. Consequently, finned structure inherently will have less form drag. This can be seen in Fig. 3, where friction factor of foams is considerable higher than for fins; especially in for higher Reynolds numbers. It can be minimized by decreasing strut cross-section, but this affects the effective thermal conductivity as will be discussed further on.

Effective Viscosity

The last additional term obtained by averaging is the Brinkman extension with effective viscosity $\underline{\underline{\mu^e}}$. It accounts for the influence of the solid matrix on boundary effects near the walls confining it. Effective viscosity is found to depend on the fluid's viscosity and the structural properties of the solid matrix [46]. Lundgren [65] gave theoretical proof for the validity of the Brinkman closure term. To quantify effective viscosity, Gilver and Altobelli [66] matched nuclear magnetic resonance data with the Brinkman model for a 0.972 porosity foam, finding an effective to molecular viscosity ration of 7.5. However, a recent study of Magnico [45] states that μ^e/μ should be between 1.75 and 2, in all the Reynolds number range. Breugem [67] on the other hand claims that for homogeneous channel-type porous media with $\phi>3/7$, this ratio is always less than 1 (i.e. $\mu^e/\mu=0.5(\phi-3/7)$). Lundgren [65] finally derived that the effective/molecular viscosity ratio is larger than one for $0.7<\phi<1$ (with a maximum of 1.25) and smaller than 1 otherwise. It is clear that no consensus on the subject is available, requiring further investigation.

Averaging the Energy Equations

Energy transport in the solid phase is different from the fluid phase, each requiring a dedicated transport equation. Applying the averaging operator on both energy equations yields [68]:

$$\phi(\rho c_p)_f\frac{\partial\langle T_f\rangle^i}{\partial t} + (\rho c_p)_f\nabla\cdot(\langle\vec{v}\rangle^s\langle T_f\rangle^i) = \nabla\cdot k_f\left[\phi\nabla\langle T_f\rangle^i+\frac{1}{V_{REV}}\int_{A_{fs}}\vec{n}_{fs}\widetilde{T}_f dA\right] -(\rho c_p)_f\nabla\cdot\langle\widetilde{\vec{v}}\widetilde{T}_f\rangle^s + k_f\frac{1}{V_{REV}}\int_{A_{fs}}\vec{n}_{fs}\cdot\nabla\widetilde{T}_f dA \quad (9)$$

$$(1-\phi)(\rho c_p)_s\frac{\partial\langle T_s\rangle^i}{\partial t} = \nabla\cdot k_s\left[(1-\phi)\nabla\langle T_s\rangle^i+\frac{1}{V_{REV}}\int_{A_{fs}}\vec{n}_{sf}\widetilde{T}_s dA\right] +k_f\frac{1}{V_{REV}}\int_{A_{fs}}\vec{n}_{sf}\cdot\nabla\widetilde{T}_s dA, \quad (10)$$

with T [K] temperature, c_p [J/kgK] specific heat and k [W/mK] thermal conductivity. The earlier introduced length scale constraint is also imposed on the averaged solid and fluid temperature fields, minimizing their respective variation in a REV.

Tortuosity

For foams, the true length of struts between two points in the solid matrix is considerably longer than the apparent length. Consequently, thermal path is longer, which results in additional conductive resistance. This is accounted for by the additional integral term in the diffusive part of the solid averaged energy equation (10). It is a correction due to the solid matrix geometry. The ratio of true versus apparent strut length is termed solid tortuosity, resulting in the additional integral term referred to as the tortuosity term. Bodla et al. [69] measured tortuosity by creating a nodal network on a µCT scan virtual foam representation. This yields values ranging from 2.15 to 3.31, depending on the foam type and the measuring direction. Brun [58] measured tortuosity in a same fashion, finding an average value of 1.33. After defining the principle axis of the cell structure, azimuth and elevation distributions could be obtained. A sinusoidal variation is observed with a period of 180 degrees, confirming the PUC representation assumption discussed in the foam geometry review. The author concludes that tortuosity is orthotropic, correlating with cell orientation. Although showing large scatter, the results indicate that the tortuosity term represents a significant correction for the solid phase thermal conductivity.

Also in the fluid phase equation (9), pure conductive heat transfer requires a correction due to a tortuous path, induced by the solid matrix. Indeed, an excessive length has been quantified via airborne ultrasound by Le et al. [70], resulting in 1.003 for a 5PPI foam with 0.95 porosity and 1.032 for a 20PPI foam with 0.88 porosity. When the solid to fluid thermal conductivity ratio is in the order of 1000 or more, the fluid tortuosity can be neglected [71]. Typical example is air in an aluminum structure. In this case, the stagnant thermal conductivity of the fluid phase equals the phase-fraction weighted fluid thermal conductivity. It should be stipulated that no hydrodynamic effects are included in this fluid tortuosity and therefore should not be confused with the definition of e.g. Du Plessis et al. [72], which is discussed later when dispersion is treated.

Solid Phase Thermal Conductivity

Schmierer et al. [10] measured the solid phase thermal conductivity in vacuum, blocking natural convection. Bhattacharya et al. [19] and Paek et al [73] did the same measurements under atmospheric conditions. In the three cases, heat was supplied on top of two samples, comprising the

unknown foam and a known material. This allows to calculate uncertainties, being 7.9% on average, 12% and 3.8% for respectively [10], [73] and [19]. For foam with 0.96 porosity, all three data sets yielded the same thermal conductivity. For lower porosities however, the results obtained under vacuum conditions are higher than in air at atmospheric pressure. Although a metallic bonding is applied (i.e. brazing), Schmierer et al. [10] contributes this difference to worse thermal contact resistance due to using less brazing material in case of [19]. Nevertheless, it can be concluded that air inside the foam structure has minimal effect on the solid thermal conductivity, i.e. when heat is applied on top of the sample and temperature difference across the sample is limited.

The results obtained by Bhattacharya et al. [19] and Paek et al. [73] are depicted in Fig. 16. The aluminium alloy in both cases is T-6101, having bulk thermal conductivity of 218 W/mK. When only a phase weighted value of the bulk material's thermal conductivity is used, a maximum stagnant thermal conductivity is reached as shown by the line in Fig. 16.

The ratio of this maximum to the real values ranges between 2.18 and 3.4, which shows great resemblance with the solid tortuosity measurement of Bodla et al. [69]. Remark that tortuosity for fins is close to 1, meaning that a minor correction on the phase weighted thermal conductivity is required. This explains the significant fin efficiency difference between foams and fins in a conventional 2D heat exchanger.

Improving thermal conductivity can be done by increasing strut cross-section, but will result in dramatic pressure drop increment as was discussed before. Besides making fin/foam combinations to increase thermal conductivity (and thus improve fin efficiency as was discussed), the only remaining solution is to minimize the conductive path which can be achieved by minimizing the distance towards the thermal boundary confining the solid matrix.

The measured thermal conductivity of the solid phase can also include radiative heat transfer. Zhao et al. [74] experimentally investigated this for FeCrAlY foam by decomposing thermal conductivity in a contribution due to the solid phase and radiation. The latter was cast in a "radiative conductivity". A temperature dependency is found, ranging from 0.05 to 0.5 $Wm^{-1}K^{-1}$ at respectively 50°C and 450°C operating temperature. For applications operating below 100°C, this contribution is 4% at most (i.e. for the highest porosities).

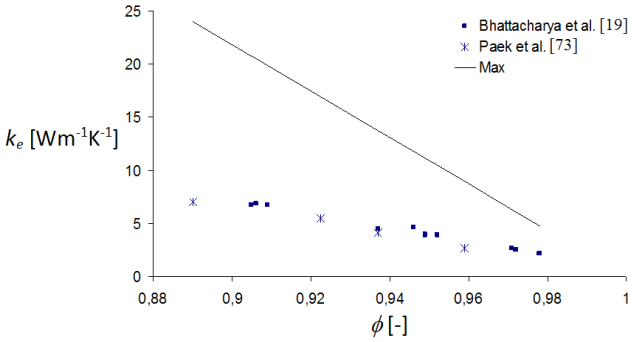

Figure 16: Experimental data of effective thermal conductivity for open-cell aluminum foam saturated with air and a maximum value obtained via phase-fraction weighting.

In order to develop a design tool for heat transfer with open-cell metal foams, thermal conductivity has to be described as a function of geometrical parameters. A variety of models are available to predict effective thermal conductivity. The first model is presented by Dul'nev [18], using a cubic cell model with struts represented by squared rods. Layering the structure allows to represent foam as a thermal resistor diagram, which can be computed via Fourier's conduction law. For higher porosities (ϕ>0.95), the model provides acceptable accuracy. The same principle is applied by Calmidi and Mahajan [75] on a two-dimensional array of hexagonal cells with squared nodes. This was further optimized to round nodes by Bhattacharya et al. [19]. The model needed to be tuned with experimental data, because struts were represented as solid cylinders with constant cross-section. This is confirmed to be an oversimplification, by Kanaun and Tkachenko [29], who found that smallest strut cross-sectional surface area, as well as its variation along the axial position in the strut have significant influence. After this tuning, the proposed model allows to predict effective thermal conductivity within experimental uncertainty for aluminum foams. They also proposed an empirical correlation based on the porosity, where the phase weighted conductivity had to be multiplied by a factor 0.35, which can be considered the inverse of average tortuosity.

Three dimensional models are commonly based on an isotropic Kelvin cell representation, where Boomsma and Poulikakos [76] used cubic nodes and Schmierer et al. [10] applied spherical nodes. Although a good correlation with their own experimental data could be obtained by [76], Dai et al. [77] found it erroneous, presenting a correction which takes strut orientation in account. Applying numerical techniques, it is possible to compute thermal conductivity of more complex models. Krishnan et al. [78] constructed a model of the solid matrix by subtracting packed spheres from the porous domain. The remainder represents the solid phase. They found that packing the spheres on an A15 lattice, it is possible to have a model which is in agreement with a wide range of porosities. The most realistic results can be obtained by solving the heat conduction equation numerically on a µCT virtual reconstruction as applied by Bodla et al. [69].

Interfacial Heat Transfer

Both last integral terms in equations (9) and (10) resemble the interfacial heat transfer between both phases, resulting from invoking continuous heat flux across the interface. A common approach is applying Newton's cooling law, where a convection coefficient is implemented to quantify the heat transfer driven by the difference between averaged solid and fluid temperature in the REV. The surface-to-volume ratio takes the interfacial surface area in account, yielding:

$$\dot{q} = h\sigma_0(\langle T_s \rangle - \langle T_f \rangle), \qquad (11)$$

Where q [W/m³] is the volumetric heat rate and h [W/m²K] is convective heat transfer coefficient. It is important to underline that the interfacial heat transfer is accounted for via a volumetric heat source or sink for both phases and does not take hydrodynamic effects in account. Most of the earlier discussed convection correlations (see Fig. 12a) are obtained in foam volumes with different sizes, where boundary effects can

have significant influence. However, the Zukauskas [40] correlation is found to be appropriate in a volume average treatment [35]. This conclusion is further supported from the measurements done by Dukhan et al. [49], who measured foam samples which can be considered infinitely high (temperature of solid is not changing and in equilibrium with fluid temperature) and confirmed the Zukauskas correlation.

Note that under certain conditions, the temperature differences between both solid and fluid phase can become negligibly small (not zero as this would imply that there is no interfacial heat transfer), which is referred to as a local thermal equilibrium approximation. This allows to combine the energy equation of both phases (9) and (10), abandoning the concept of the convective heat transfer coefficient. According Kaviany [46], the assumption of local thermal equilibrium requires that the sub-REV scale, local temperature differences between solid and fluid phase are smaller than the temperature difference over a REV, which in turn has to be considerable smaller than the temperature difference over the foam volume. The thermal conductivity then becomes a weighted average of both phases, with their respective corrections. However, there is are still hydrodynamics effects which occur on sub-pore scale level and treated next.

Thermal Dispersion

The second to last term in equation (9) results from the local velocity variation in the REV and is called thermal dispersion. This describes the spreading of heat due to the deviation of local velocity from the REV average. It is purely triggered by the presence of the solid matrix. Streamlines are split and subsequently united, when passing by a strut. This allows different streamlines to mix and is therefore also referred to as mechanical dispersion. However, when the convective forces inside the foam pores overwhelm the momentum diffusion, turbulence can be triggered, resulting in additional mixing. This is treated separately and specifically termed turbulent dispersion.

Elaborating on the mechanical dispersion, the hydrodynamic mixing effects are commonly modelled by a diffusion-gradient type equation which is given by:

$$-(\rho c_p)_f \nabla \cdot \langle \widetilde{v}\widetilde{T}_f \rangle^s = \underline{\underline{K_d}} \nabla \langle T_f \rangle^i \qquad (12)$$

where $\underline{\underline{K_d}}$ represents the dispersion tensor. It is expected to be influenced by the flow conditions (Reynolds number), ratio of viscous to thermal boundary layer (Prandtl number), solid to fluid thermal diffusion coefficient and structural parameters of the solid matrix. Calmidi and Mahajan [35] proposed following correlation:

$$k_d/k_e = C_D \, Re_K Pr_e \,, \qquad (13)$$

with k_e the stagnant thermal conductivity and C_D is a constant which has been determined experimentally to be 0.06. For relatively low air velocities (3m/s) through a 0.95 porosity foam, the dispersion conductivity is merely 3% of the stagnant thermal conductivity. For air velocities up to 20m/s, dispersion becomes 27%. Remark however that dispersion behaves tensorial, which is clearly illustrated by Alshare et al. [79]. Stream-wise dispersion is found to be two orders of magnitude larger than cross-stream dispersion. This was confirmed by Yang and Nakayama [80]. However, like for momentum dispersion, further investigation is also required for the thermal dispersion.

FOAM IN THERMAL APPLICATIONS

Potential heat transfer applications have emerged during last decade. For military use, laboratory scale test models showed a potential weight and size reduction in naval aircraft liquid and electronics cooling systems when applying foam instead of conventional fins in heat exchangers [81]. In aerospace applications, inserting metal foam in the cooling jackets of propulsion rocket nozzles is found to be beneficial [82] [83]. Also for the thermal protection of hypersonic and re-entry vehicles, aluminum foam sandwich panels are looking promising [41]. A major advantage is a homogeneous velocity distribution of the coolant in the foam, reducing hot spots. In a turbojet engine, placing a ring of foam between the combustor and turbine section gave promising results as this homogenized the temperature leaving the combustor which raises the engine's overall efficiency [84]. Another possibility to improve efficiency is a variable cycle engine, for which an additional heat exchanger needs to be integrated in the engine which seems feasible with foam [85].

In industry, a better reaction control in a chemical reactor can be achieved by using a foam compact heat exchanger [86] because foams combines good thermal properties with very good micro-mixing. Metal foam reactors are also found to intensify the synthesis of biodiesel in such a way that small fuel processing plants for distribution purposes are possible [87]. In the mentioned applications, foams are not only used for their promising thermal properties, but also because of the mechanical dispersion. The latter makes foams excellent static mixers.

With HVAC applications in mind, porous fins are compared with conventional louvered fins yielding similar thermal performance but slightly worse pressure drop performance [56]. Dai et al. [88] on the other hand reported that a foam heat exchanger can be significantly smaller in volume and lighter in weight over a wide range of design space. The latter considered cost aspects, stating that if the price of metal foam is reduced to roughly $16/kg, the cost of the louver fin and foam heat exchangers would be equal for the baseline conditions of their study. Prototype metal foam condensers for miniature-scale refrigeration systems were build and decreased thermal resistance compared to plain fin condensers with similar characteristics, for a fixed pumping power [89]. Ghosh [90] compared foam with offset strip and wavy fins, based on the area goodness factor (j/f). Decreasing pore density increased the area goodness factor to outperform both fin types, but of course also reduces heat transfer surface area which could penalize compactness.

This demonstrates the need for optimizing the foam structure to the intended application's constraints. As strut thickness influences the thermal conductivity (or fin efficiency) and pressure drop (inertial coefficient), it suggests that depending on the application, an optimal strut dimension should exist for a given cell size which balances thermal performance and pressure drop. This is demonstrated in Fig. 17 for a compact heat exchanger with 4.85mm distance between

flat tubes and under the restriction of 300Pa pressure drop. The truncations of the surface response is based on porosity.

Foams with porosity lower than 0.75 or higher than 0.98 are considered unrealistic and therefore removed. It clearly shows that for any average cell diameter there exists an optimal strut dimension. Furthermore, there seems to be a general optimum. However, the strut dimensions are around 100µm, for average cell diameter of 1mm. From manufacturing point of view, these structures are not feasible with the discussed investment casting process.

Replacing conventional finned heat sinks with foam heat sinks can be seen as a high potential application. Kim et al. [91] compared different foams with conventional fin heat sinks of the same size, both filling half the channel height. Transversal air flow experiments showed an increased thermal performance of more than 28%, only weighting 25% of the fin heat sinks. Mixed convection in the same configuration, but with multiple porous volumes placed at the bottom of the channel can reduce the maximum temperature in electronics by 50% [92]. For the characterization of heat sinks filling the complete channel height, an increase in the range of 30% is reported [93] when comparing foam and straight fin heat sinks for a given fan power.

The typical impinging flow in electronics cooling, instead of parallel to the heat sink base, is characterized by Hsieh et al. [94]. Controlling the air flow entering the top of foam heat sinks, yields Nusselt number correlations for six types of aluminum foams. Visualization of a single round jet impinging on metal foam helps to understand the influence of permeability on jet flow penetration, aiding the design of more effective foam heat sinks [95]. Finally, concerning potential heat sink applications, porous pin fin heat sinks are reported to have significant heat transfer enhancement and pressure drop reduction [80].

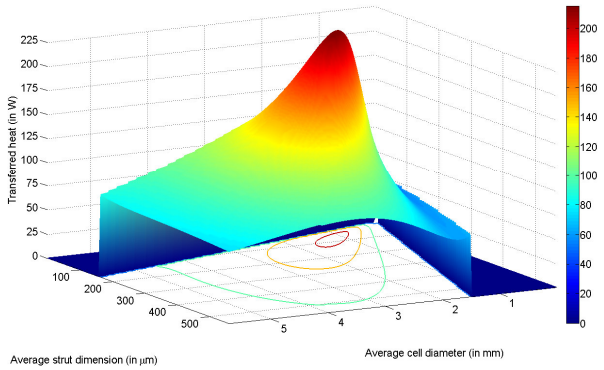

Figure 17: Heat transfer for various structural foam configurations for a fixed tube pitch and pressure drop.

CONCLUSIONS

Key to analyzing the thermal and hydraulic behaviour of a metal foam is to have an unambiguous geometrical model as it significantly influences flow behaviour. The latter is directly linked to heat transfer and pressure drop. A proposal for a general foam model is discussed.

Classical heat transfer theory and coefficients have been employed for a variety of foam structures and flow arrangements. This black-box treatment, and the fact that a large number of geometrical parameters have been defined, results in largely deviating results. Nevertheless, from these analysis, it can be concluded that in conventional heat transfer configurations, the convective heat transfer with open-cell metal foams is considerably better than for fins because the structure simple does not allow the formation of large boundary layers. However, to be able to use foam in compact heat exchangers, surface-to-volume ratio and fin effectiveness needs also to be sufficient. Foams can reach $900m^{-1}$ when uncompressed, which is rather on the low side when comparing with the standard $1500m^{-1}$ used in fin structures. Also for fin effectiveness, relatively low values (0.78 versus minimum 0.89 for respectively foam and fins) have been reported.

A second method to analyze foam is directly solving the conservation laws, but this is only applicable on a limited foam volume due to computational constraints. This multi-scale issue can be overcome via local volume averaging. However, this introduces the so called macroscopic properties, which transport microscopical phenomena to the averaged dimensions. Closing the momentum equation introduces the permeability and inertial loss factor, which both have been discussed extensively in literature. A third property which takes the no-slip condition of the walls confining the solid matrix in account, namely effective viscosity, has not been closed conclusively.

Closing the energy equation for the general case of local thermal non-equilibrium introduced solid phase thermal conductivity. This can be considered the Achilles heel of foam for heat transfer applications, which was also observed via black-box treatment as the relatively limited fin efficiency. The main reason is the tortuous thermal path in the solid phase. Solutions have been proposed by either using “thermal path enhancing”, i.e. using a fin/foam combination or minimizing the tube pitch when e.g. flat tubes are used.

When examining thermal performance for a given pressure drop, it becomes clear that there is a trade-off which needs to be made. Thicker struts will enhance thermal conductivity and thus heat transfer, but on the other hand increase the pressure drop penalty. It suggest the existence of an optimum for given flow arrangement and operating conditions. However, further investigation is required to come to actual design criteria.

Interfacial heat transfer is treated via Newton’s cooling law, where a convection coefficient acts on the difference between averaged solid and fluid temperature in the REV. Foams are treated as external flow around pins, for which the Zukauskas correlation is considered a reference. It has been confirmed that this correlation indeed yields viable results for foams.

Additionally to the interfacial heat transfer, there is thermal dispersion which takes hydrodynamic mixing in account. Streamlines are split and subsequently united to pass a strut. This mechanism allows for additional mixing. Analogue to turbulence modelling, a diffusion-gradient type model is used. A proportionality constant is introduced (thermal dispersion) which relates the hydrodynamic mixing to the gradient of averaged fluid temperature. Closure models for this constant have been proposed, but show significant scatter. Further investigation is required.

ACKNOWLEDGEMENT

The authors express their gratitude to Bekaert for the close cooperation and greatly acknowledge the "IWT Vlaanderen" for their financial support (IWT-090273).

NOMENCLATURE

A_{sf}	[m²]	Interfacial surface area
A_0	[m²]	Strut cross-sectional surface area
A	[m²]	Surface area
a_1	[-]	Strut cross-sectional shape factor
a_2	[-]	Strut axial shape factor
b	[m]	Distance between two tubes
C_D	[-]	Thermal dispersion coefficient
c_p	[J/kgK]	Specific heat
d_1	[m]	Transverse diameter of ellipse encompassing a cell
d_2	[m]	Conjugate diameter of ellipse encompassing a cell
d_p	[m]	Pore diameter
d_s	[m]	Equivalent strut diameter yielding same A_0
$\vec{g}$	[m/s²]	Gravitational acceleration
h	[W/m²K]	Convection coefficient
j	[-]	Colburn j factor
$\underline{\underline{K_d}}$	[W/mK]	Thermal dispersion tensor
k	[W/mK]	Thermal conductivity
L	[m]	Flow length through foam
l	[m]	Length
P	[Pa]	Pressure
$\dot{q}$	[W/m³]	Volumetric heat rate
Re	[-]	Reynolds number
r_0	[m]	Characteristic dimension REV
$\vec{r}$	[m]	Local position
T	[K]	Temperature
t	[s]	Time
V	[m³]	Volume
$\vec{v}$	[m/s]	Velocity
x,y,z	[m]	Cartesian coordinates

Special characters

Φ	[-]	Porosity
ρ_r	[-]	Relative density
σ_0	[m^{-1}]	Surface-to-volume ratio
ξ	[-]	Relative strut length
θ	[°]	Louver angle
δ	[m]	Fin thickness
ψ	[-]	Arbitrary quantity
ρ	[kg/m³]	Density
μ	[Pa.s]	Viscosity
$\underline{\underline{\kappa}}$	[m²]	Permeability
$\underline{\underline{\beta}}$	[-]	Inertial coefficient

Subscripts

f	Fluid phase
REV	Representative Elementary Volume
s	Solid phase
sf	Solid-fluid interface

Superscripts

e	Effective property
i	Intrinsic average
s	Superficial average

REFERENCES

[1] Ashby M.F., Evans A., Fleck N., Gibson L.J., Hutchinson J., Wadley H., Metal Foams: A Design Guide, Butterworth-Heinemann Publications, Woburn MA, USA, 2000.

[2] Tian J., Lu T., Hodson H.P., Queheillalt D., Wadley H., Cross flow heat exchange of textile cellular metal core sandwich panels, *International Journal of Heat and Mass Transfer,* Vol. 50, 2007, pp. 2521-2536.

[3] Banhart J., Manufacture, characterisation and application of cellular metals and metal foams, *Progress in Materials Science*, Vol. 46, No. 6, 2001, pp. 559-632.

[4] Walz D.D., Cordova R., Method of making an inorganic reticulated foam structure, *Energy Research Generation Inc.*, Oakland, Ca, USA, 1967.

[5] Sekulic D.P., Dakhoul Y.M., Zhao H., Liu W., Aluminum foam compact heat exchangers: brazing technology vs. thermal performance, *Proceedings of the Cellmet 2008 Conference*, 2008.

[6] Turrif D., Corbin S., Kozdras M., Diffusional solidification phenomena in clad aluminum automotive braze sheet, *Acta Materialia*, Vol. 58, No. 4, 2010, pp. 1332-1341.

[7] Perrot C., Panneton R., Olny X., Periodic unit cell reconstruction of porous media: Application to open-cell aluminum foams, *Journal of Applied Physics*, Vol. 101, No. 11, 2007, pp. 1-11.

[8] Zhou J., Mercer C., Soboyejo W., An investigation of the microstructure and strength of open-cell 6101 aluminum foams, *Metallurgical and Materials Transactions*, Vol. 33, No. 5, 2002, pp. 1413-1427.

[9] Gibson L.J., Ashby M.F., Cellular Solids: Structure and Properties, Cambridge University Press, Cambridge, U.K., second edition, 1997.

[10] Schmierer E.N., Razani A., Self-consistent open-celled metal foam model for thermal applications, *Journal of Heat Transfer*, Vol. 128, No. 11, 2006, pp. 1194-1203.

[11] T'Joen C., De Jaeger P., Huisseune H., Van Herzeele S., Vorst N., De Paepe M., Thermo-hydraulic study of a single row heat exchanger consisting of metal foam covered round tubes, *International Journal of Heat and Mass Transfer*, Vol. 53, No. 15, 2010, pp. 3262-3274.

[12] Bonnet J.P., Topin F., Tadrist L., Flow laws in metal foams: Compressibility and pore size effects, *Transport in Porous Media*, Vol. 73, No. 2, 2008, pp. 233-254.

[13] Ozmat B., Leyda B., Benson B., Thermal applications of open-cell metal foams, *Materials and Manufacturing Processes*, Vol. 19, No. 5, 2004, pp. 839-862.

[14] Sing K., Everett D., Haul R., Moscou L., Pierotti R., Rouquerol J., Siemieniewska T., IUPAC Recommendations 1984: reporting physisorption data for gas/solid systems with special reference to the determination of surface area and porosity, *Pure Applied Chemistry*, Vol. 57, No. 4, 1985, pp. 603-619.

[15] Vlassenbroeck J., Dierick M., Masschaele B., Cnudde V., Van Hoorebeke L., Jacobs P., Software tools for quantification of X-ray microtomography at the UGCT, *Nuclear Instruments and Methods in Physics Research Section A: Accelerators, Spectrometers, Detectors and Associated Equipment,* Vol. 580, No. 1, 2007, pp. 442-445.

[16] Tadrist L., Miscevic M., Rahli O., Topin F., About the use of fibrous materials in compact heat exchangers, *Experimental Thermal and Fluid Science*, Vol. 28 No. 2, 2004, pp. 193-199.

[17] Hugo J., Topin F., Tadrist L., Brun A., From pore scale numerical simulation of conjugate heat transfer in cellular material to effective transport properties of real structures, *Proceedings of the 14th International Heat Transfer Conference (IHTC)*, 2010.

[18] Dul'nev G.N., Heat transfer through solid disperse systems, *International Journal of Engineering Physics and Thermophysics*, Vol. 9, No. 3, 1965, pp. 399-404.

[19] Bhattacharya A., Calmidi V.V., Mahajan R.L., Thermophysical properties of high porosity metal foams, *International Journal of Heat and Mass Transfer*, Vol. 45, No. 5, 2002, pp. 1017-1031.

[20] Lu T.J., Stone H.A., Ashby M.F., Heat transfer in open-cell metal foams, *Acta Materialia*, Vol. 46, No. 10, 1998, pp. 3619-3635.

[21] Dharmasena K., Wadley H., Electrical conductivity of open-cell metal foams, *Journal of Material Research*, Vol. 17, No. 3, 2002, pp. 625-631.

[22] Ghosh I., Heat-transfer analysis of high porosity open-cell metal foam, *Journal of Heat Transfer*, Vol. 130, 2008

[23] Weaire D., Phelan R., A counter-example to Kelvin's conjecture on minimal surfaces, *Philosophical Magazine Letters*, Vol. 69, No. 2, 1994, pp. 107-110.

[24] Brakke K., The surface evolver, *Experimental Mathematics,* Vol. 1, No. 2, 1992, pp. 141-165.

[25] Lautensack C., Sych T., 3D image analysis of open foams using random tessellations, *Image Analysis and Stereology*, Vol. 25, 2006, pp. 87-93.

[26] Sullivan J.M., The geometry of bubbles and foams, *Foams and Emulsions*, 354, 1998, pp. 379-402.

[27] Hutter C., Zenklusen A., Kuhn S., Rudolf von Rohr P., Large eddy simulations of flow through a streamwise-periodic structure, *Chemical Engineering Science*, 2010.

[28] Redenbach C., Modelling foam structures using random tessellations, *Proceedings of the 10th European Congress of International Society for Stereology*, 2009.

[29] Kanaun S., Tkachenko E., Effective conductive properties of open-cell foams, *International Journal of Engineering Science*, Vol. 46, No. 6, 2008, pp. 551-571.

[30] Kopanidis A., Theodorakakos A., Gavaises E., Bouris D., 3D numerical simulation of flow and conjugate heat transfer through a pore scale model of high porosity open cell metal foam, *International Journal of Heat and Mass Transfer*, Vol. 53, No. 11, 2010, pp. 2539-2550.

[31] Edouard D., Lacroix M., Huu C.P., Luck F., Pressure drop modeling on SOLID foam: State-of-the art correlation, *Chemical Engineering Journal*, Vol. 144, No. 2, 2008, pp. 299-311.

[32] Jang W., Kraynik A., Kyriakides S., On the microstructure of open-cell foams and its effect on elastic properties, *International Journal of Solids and Structures*, Vol. 45, No. 7, 2008, pp. 1845-1875. [33] Shah R.K., Sekulic D.P., Fundamentals of Heat Exchanger Design, John Wiley & Sons, Inc., Hoboken, NJ, US, 2003.

[34] Hwang J.J., Hwang G.J., Yeh R.H., Chao C.H., Measurement of interstitial convective heat transfer and frictional drag for flow across metal foams, *Journal of Heat Transfer*, Vol. 124, 2002, pp. 120-129.

[35] Calmidi V.V., Mahajan R.L., Forced convection in high porosity metal foams, *Journal of Heat Transfer*, Vol. 122, No. 3, 2000, pp. 557-565.

[36] Wang C.C., Lee C.J., Chang C.T., Lin S.P., Heat transfer and friction correlation for compact louvered fin-and-tube heat exchangers, *International Journal of Heat and Mass Transfer*, Vol. 42, No. 11, 1998, pp. 1945-1956.

[37] Kuwahara F., Shirota M., Nakayama A., A numerical study of interfacial convective heat transfer coefficient in two-energy equation model for convection in porous media, *International Journal of Heat and Mass Transfer*, Vol. 44, 2001, pp. 1153-1159.

[38] Giani L., Groppi G., Tronconi E., Mass-transfer characterization of metallic foams as supports for structured catalysts, *Industrial & Engineering Chemistry Research*, Vol. 44, No. 14, 2005, pp. 4993-5002.

[39] Kamiuto K., Yee S.S., Heat transfer correlations for open-cellular porous materials, *International Communications in Heat and Mass Transfer*, Vol. 32, No. 7, 2005, pp. 947-953.
[40] Zhukauskas A.A., Convective heat transfer in cross-flow. In: Kakac S., Shah R.K., Aung W., Editors, Handbook of single-phase convective heat transfer, Wiley, New York, 1987.
[41] Salas K.I., Waas A.M., Convective heat transfer in open cell metal foams, *Journal of Heat Transfer*, Vol. 129, No. 9, 2007, pp. 1217-1230.
[42] Liu J.F., Wu W.T., Chiu W.C., Hsieh W.H., Measurement and correlation of friction characteristic of flow through foam matrixes, *Experimental Thermal and Fluid Science*, Vol. 30, No. 4, 2006, pp. 329-336.
[43] Dukhan N., Patel P., Equivalent particle diameter and length scale for pressure drop in porous metals, *Experimental Thermal and Fluid Science*, Vol. 32, No. 5, 2008, pp. 1059-1067.
[44] Petrasch J., Meier F., Friess H., Steinfeld A., Tomography based determination of permeability, Dupuit-Forchheimer coefficient, and interfacial heat transfer coefficient in reticulate porous ceramics, *International Journal of Heat and Fluid Flow*, Vol. 29, No. 1, 2008, pp. 315-326.
[45] Magnico P., Analysis of permeability and effective viscosity by CFD on isotropic and anisotropic metallic foams, *Chemical Engineering Science*, Vol. 64, No. 16, 2009, pp. 3564-3575.
[46] Kaviany M., Principles of Heat Transfer in Porous Media, Mechanical Engineering Series, Springer-Verlag New York, Inc., second edition edn., 1995.
[47] Miwa S., Revankar S.T., Hydrodynamic Characterization of Nickel Metal Foam, Part 1: Single-Phase Permeability, *Transport in Porous Media*, Vol. 80, No. 2, 2009, pp. 269-279.
[48] Lu W., Zhao C.Y., Tassou S.A., Thermal analysis on metal-foam filled heat exchangers. Part I: Metal-foam filled pipes, *International Journal of Heat and Mass Transfer*, Vol. 49, No. 15, 2006, pp. 2751-2761.
[49] Dukhan H., Quinones-Ramos P.D., Cruz-Ruiz E., Velez-Reyes M., Scott E.P., One-dimensional heat transfer analysis in open-cell 10-ppi metal foam, *International Journal of Heat and Mass Transfer*, Vol. 48, 2005, pp. 5112-5120.
[50] Dukhan N., Picon-Feliciano R., Alvarez-Hernandez A.R., Heat transfer analysis in metal foams with low-conductivity fluids, *Journal of Heat Transfer,* Vol. 128, 2006, pp. 784-792.
[51] Alvarez-Hernandez A.R., Combined Flow and Heat Transfer Characterization of Open Cell Aluminum Foams, Master's thesis, University of Puerto Rico Mayaguez Campus, 2005.
[52] Shah R.K., Compact heat exchangers for microturbines, *Proceedings of fifth International Conference on Enhanced, Compact and Ultra-Compact heat Exchangers: Science and Technology*, pp. 247-257.
[53] Bhattacharya A., Mahajan R.L., Finned metal foam heat sinks for electronics cooling in forced convection, *Journal of Electronic Packaging*, Vol. 124, 2002, pp. 155-163.
[54] Seyf H.R., Layeghi M., Numerical analysis of convective heat transfer from an elliptic pin fin heat sink with and without metal foam insert, *Journal of Heat Transfer*, Vol. 132, 2010.
[55] Shih W.H., Chou F.C., Hsieh W.H., Experimental investigation of the heat transfer characteristics of aluminum-foam heat sinks with restricted flow outlet, *Journal of Heat Transfer*, Vol. 129, 2007.
[56] Kim S.Y., Paek, J.W., Kang, B.H., Flow and heat transfer correlations for porous fin in a plate-fin heat exchanger, *Journal of Heat Transfer*, Vol. 122, pp. 572-578.
[57] Whitaker S., The method of volume averaging, *Theory and Application of Transport in Porous Media*, Vol. 13, 2010.
[58] Brun E., De l'imagerie 3D des structures a l'étude des mécanismes de transport en miliuex cellulaires, Ph.D. thesis, 2009.
[59] Whitaker S., The Forchheimer equation: A theoretical development, Vol. 25, 1996, No. 1, pp. 27-61.
[60] Mahjoob S., Vafai K., A synthesis of fluid and thermal transport models for metal foam heat exchangers, *International Journal of Heat and Mass Transfer*, Vol. 51, 2008, pp. 3701-3711.
[61] Seguin D., Montillet A., Comiti J., Huet F., Experimental characterization of flow regimes in various porous media – II : Transition to turbulent regime, *Chemical Engineering Science*, Vol. 53, No. 22, 1998, pp. 3897-3909.
[62] Hlushkou D., Tallarek U., Transition from creeping via viscous-inertial to turbulent flow in fixed beds, *Journal of Chromotography*, Vol. 1126, 2006, pp. 70-85.
[63] Dukhan N., Minjeur C.A., A two-permeability approach for assessing flow properties in metal foam, *Journal of Porous Material* 2010, pp. 1-8.
[64] Innocentini M.D.M., Lefebvre L.P., Meloni R.V., Baril E., Influence of sample thickness and measurement set-up on the experimental evaluation of permeability of metallic foams, *Journal of Porous Materials,* 2010, pp. 491-499.
[65] Lundgren, T.S.: Slow flow through stationary random beds and suspensions of spheres. *Journal of Fluid Mechanics*, Vol. 51, 1972, pp. 273–299.
[66] Givler R.C., Altobelli S.A., A determination of the effective viscosity for the Brinkman–Forchheimer flow model, *Journal of Fluid Mechanics*, Vol. 258, 1994, pp. 355.
[67] Breugem W.P., The effective viscosity of a channel-type porous medium, *Physics of Fluids*, Vol. 19, 2007, No. 10.
[68] Quintard M., Kaviany M., Whitaker S., Two-medium treatment of heat transfer in porous media: numerical results for effective properties, *Advances in Water Resources*, Vol. 20, No. 2, 1997, pp. 77-94.
[69] Bodla K.K., Murthy J.Y., Garimella S.V., Microtomography-based simulation of transport through open-cell metal foams, *Numerical Heat Transfer, Part A,* Vol. 58, 2010, pp. 527-544.
[70] Le L.H., Zhang C., Ta D., Lou E., Measurement of tortuosity in aluminum foams using airborne ultrasound, *Ultrasonics*, Vol. 50, 2010, pp. 1-5.
[71] Vafai K., Handbook of Porous Media, 2000.
[72] Du Plessis P., Montillet A., Comiti J., Legrand J., Pressure drop prediction for flow through high porosity metallic foams, *Chemistry Engineering Science*, Vol. 57, 2002, pp. 2781-2789.
[73] Paek J.W., Kang B.H., Kim S.Y. Hyun J.M., Effective thermal conductivity and permeability of aluminum foam materials, *International Journal of Thermophysics*, Vol. 21, No. 2, 2000, pp. 453-464.
[74] Zhao C.Y., Lu T.J., Hodson H.P., Thermal radiation in ultralight metal foams with open cells, *International Journal of Heat and Mass Transfer*, Vol. 47, 2004, pp. 2927-2939.
[75] Calmidi V.V., Mahajan R.L., The effective thermal conductivity of high porosity fibrous metal foams, Journal of Heat Transfer, Vol. 121, 1999, pp. 466-471.
[76] Boomsma k., Poulikakos D., On the effective thermal conductivity of a three-dimensional structured fluid-saturated metal foam, *International Journal of Heat and Mass Transfer,* Vol. 44, 2001, pp. 827-836.
[77] Dai Z., Nawaz K., Park Y.G., Bock J., Jacobi A.M., Correcting and extending the Boomsma-Poulikakos effective thermal conductivity model for three-dimensional, fluid-saturated metal foams, *International Journal of Heat and Mass Transfer,* Vol. 37, 2010, pp. 575-580.
[78] Krishnan S., Murthy J.Y., Garimella S.V., Direct simulation of transport in open-cell metal foam, *Journal of Heat Transfer*, Vol. 128, 2006, pp. 793-799.
[79] Alshare A.A., Strykowski P.J., Simon T.W., Modeling of unsteady and steady fluid flow, heat transfer and dispersion in porous media using unit cell scale, *International Journal of Heat and Mass Transfer*, Vol. 53, 2010, pp. 2294-2310.
[80] Yang C., Nakayama A., A synthesis of tortuosity and dispersion in effective thermal conductivity of porous media, *International Journal of Heat and Mass Transfer*, Vol. 53, 2010, pp. 3222-3230.
[81] Klein J., Arcas N., Gilchrist G., Shields W., Yurman R., Whiteside J., Thermal management of airborne early warning and electronic warfare systems using foam metal fins, *Technology Review Journal*, 2003, pp. 103-127.
[82] Avenall R.J., Use of metallic foams for heat transfer enhancement in the cooling jacket of a rocket propulsion element, Master's Thesis, University of Florida, 2004.
[83] Bai M., Numerical evaluation of heat transfer and pressure drop in open cell foams, Master's Thesis, University of Florida, 2007.
[84] Azzi W., Roberts W.L., Rabiei A., A study on pressure drop and heat transfer in open cell metal foams for het engine applications, *Materials and Design*, Vol. 28, 2007, pp. 569-574.
[85] Geiger D., An experiment on integrated thermal management using metallic foams, Master's Thesis, California Polytechnic State University, 2009.
[86] Ferrouillat S., Tochon P., Peerhossaini H., Micromixing enhancement by turbulence: Application to multifunctional heat exchangers, *Chemical Engineering and Processing*, Vol. 45, 2006, pp. 633-640.
[87] Yu X.H., Wen Z.Z., Lin Y., Tu S.T., Wang Z.D. Yan J.Y., Intensification of biodiesel synthesis using metal foam reactors, *Fuel*, Vol. 89, 2010, pp. 3450-3456.
[88] Dai Z., Nawaz K., Park Y., Chen Q., Jacobi A.M., A comparison of metal-foam heat exchangers to compact multi-louver designs for air-side heat transfer applications, *Proceedings of the Seventh International Conference on Enhanced, Compact and Ultra-Compact Heat Exchangers,* 2009, pp. 49-57.
[89] Ribeiro G.B., Barbosa J.R., Prata A.T., Metal foam condensers for miniature-scale refrigeration systems, *Proceedings of the Seventh World Conference on Experimental Heat Transfer, Fluid Mechanics and Thermodynamics,* 2009, pp. 483-490.
[90] Ghosh I., How good is open-cell metal foam as heat transfer surface?, *Journal of Heat Transfer*, Vol. 131, 2009.
[91] Kim Y., Paek J.W., Kang B.H., Thermal performance of aluminium-foam heat sinks by forced air cooling, *IEEE Transactions on Components and Packaging Technologies*, Vol. 26, No. 1, 2003, pp. 262-267.
[92] Rachedi R., Chikh S., Enhancement of electronic cooling by insertion of foam materials, *Heat and Mass Transfer*, Vol. 37, 2001, pp. 371-378.
[93] Hernández A.R.A., Combined flow and heat transfer characterization of open cell aluminum foams, Master's Thesis, University of Puerto Rico, 2005.
[94] Hsieh W.H., Wu J.Y., Shih W.H., Chiu W.C., Experimental investigation of heat-transfer characteristics of aluminum-foam heat sinks, *International Journal of Heat and Mass Transfer,* Vol. 47, 2004, pp. 5149-5157.
[95] Yakkatelli R., Wu Q.H., Fleischer A., A flow visualization study of the jet dynamics in a round jet impinging on a foamed aluminum porous media, *Proceedings of International Mechanics Engineering Congress and Exposition*, 2008, pp. 977-981.